Nanomaterials

DOI: 10.1002/anie.201202244

Nanoparticulate Iron Oxide Tubes from Microporous Organic Nanotubes as Stable Anode Materials for Lithium Ion Batteries**

*Narae Kang, Ji Hoon Park, Jaewon Choi, Jaewon Jin, Jiseul Chun, Il Gu Jung, Jaehong Jeong, Je-Geun Park, Sang Moon Lee, Hae Jin Kim, and Seung Uk Son**

During the last several decades, diverse porous materials have been prepared for a wide range of applications, such as adsorbents, gas storage materials, and solid supports for catalytic materials.[1–6] These materials can be classified into three groups according to their components: inorganic materials,[2] metal–organic composites,[3] and purely organic systems.[4] Among these porous materials, organic porous materials have recently attracted special attention because of their low densities and robustness.[4–6] The accumulated organic synthetic methods can also be easily applied for the designed synthesis of organic porous materials with tailored functionalites.[5] Thus, in a short period, diverse microporous organic networks have been prepared through diverse C–C bond-forming reactions.[4–6]

In the synthesis of porous organic networks, the rigid building blocks are chosen so that the connection of these building blocks through covalent bonds induces the intrinsic porosity of the materials.[4–6] Related studies have focused on the inner porosity and the resultant high surface area of materials. However, porous organic systems with well-defined outer shapes are rare.[6] In particular, the template-free synthesis of hollow organic materials is quite rare. It is noteworthy that in the synthesis of secondary target inorganic materials using porous materials, the organic templates can be easily removed by combustion in air. In these cases, the outer shapes of materials along with their inner porosity are very critical for obtaining well-defined materials. Moreover, inorganic materials with a particulate surface could be obtained from the microporosity of organic network.

[*] N. Kang, Dr. J. H. Park, J. Choi, J. Jin, J. Chun, Dr. I. G. Jung, Prof. S. U. Son
Department of Chemistry and Department of Energy Science
Sungkyunkwan University, Suwon 440-746 (Korea)
E-mail: sson@skku.edu
J. Jeong, Prof. J.-G. Park
Department of Physics & Astronomy, Seoul National University
Seoul 151-747 (Korea)
Dr. S. M. Lee, Dr. H. J. Kim
Korea Basic Science Institute
Daejeon 350-333 (Korea)

[**] This work was supported by grants NRF-2009-0084799 and the WCU program through the NRF of Korea funded by MEST (R31-2008-000-10029-0). J.H.P. is grateful for grant NRF-2010-0029698 (Priority Research Centers Program). H.J.K. is grateful for KBSI grant P30402 and the Hydrogen Energy R&D Center, a 21st century Frontier R&D Program.

Supporting information for this article is available on the WWW under http://dx.doi.org/10.1002/anie.201202244.

Recently, Cooper and others have shown that Sonogashira coupling between alkynes and arylhalides is a very efficient method for the preparation of microporous organic materials.[7] The resultant materials themselves showed promising gas-adsorption capacities. It can be expected that more diverse functional sites can be introduced into materials by designing the organic building blocks. During our trials for introduction of viologen groups into microporous organic materials, we observed the unexpected formation of microporous organic nanotubes. Herein, we present the preparation of microporous organic nanotubes and the template synthesis of iron oxide nanotubes with particulate walls and their application as anode materials for high-performance lithium ion batteries.

Figure 1a shows the synthesis of microporous organic nanotubes (MONTs). For preparation of the MONT, two building blocks, *N*,*N*′-di(4-iodophenyl)-4,4′-bipyridinium dichloride (2 equiv)[8] and tetra(4-ethynylphenyl)methane (1 equiv)[9] were dissolved in a 3:2:2 mixture of toluene, methanol, and triethylamine. After adding catalytic amount of bis(triphenylphosphine)palladium dichloride and copper iodide, the reaction mixture was heated at 90 °C for 72 h to form precipitates. After cooling to room temperature, the solid was retrieved by centrifugation and washed with excess dimethyl sulfoxide, methanol, dichloromethane, and diethyl ether. The resultant materials were dried under a vacuum for a day. The obtained precipitates were investigated by scanning electron microscopy (SEM) and transmission electron microscopy (TEM).

As shown in typical SEM images(Figure 1b), the obtained materials have a 1D character with mild ending-parts. Interestingly, a careful investigation of the materials by TEM revealed the hollow inner space and dark-contrasted walls (Figure 1c–e; Supporting Information, Figure S1). The average diameter and thickness of the wall of MONT were (92 ± 19) nm and (31 ± 4) nm, respectively. Brunauer–Emmett–Teller (BET) analysis showed the microporous character of materials with type I N_2 isotherm at 77 K, 765.0 $m^2 g^{-1}$ surface area, and 1.01 $cm^3 g^{-1}$ pore volume (P/P_0=0.995; Figure 2a). Powder X-ray diffraction (PXRD) studies revealed the amorphous character of MONT that has been observed previously[7] (Supporting Information, Figure S2). Thermogravimetric analysis (TGA) of the materials showed that they are stable up to 205 °C and then slowly decomposed at a higher temperature (Figure 2b).[10] Solid-state ^{13}C NMR spectroscopy showed signals at $\delta = 62$ ppm, $\delta = 90$ ppm, and $\delta = 120$–160 ppm for benzyl, alkyne, and aryl groups, respectively (Figure 2c). Elemental analysis of mate-

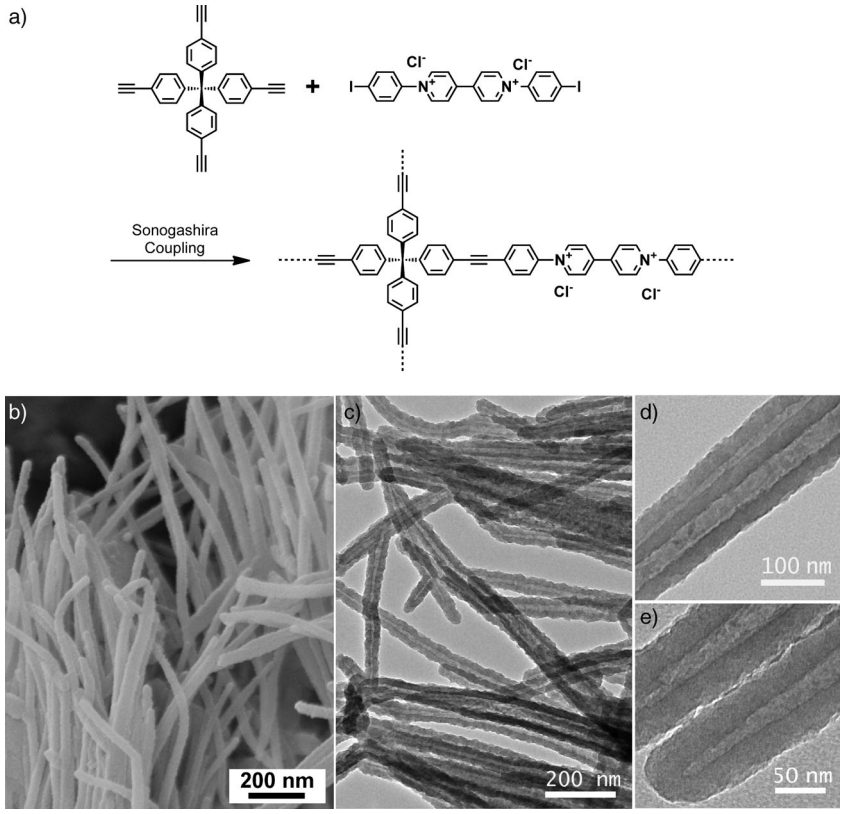

Figure 1. a) Synthesis of microporous organic nanotubes (MONTs); b) SEM image; c–e) TEM images of MONTs.

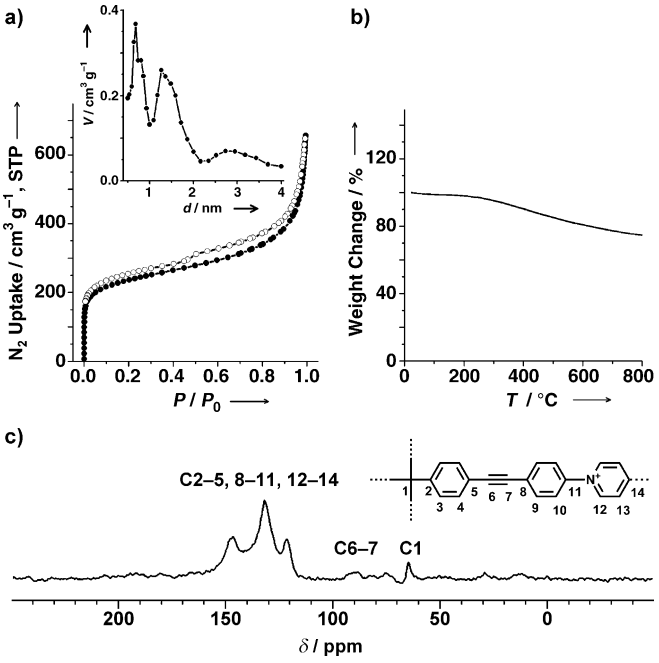

Figure 2. a) BET N_2 isotherm; inset: pore-size distribution (V = differential pore volume, d = pore size) based on the DFT method; b) TGA curve under N_2; c) solid-state ^{13}C NMR spectrum of the MONT.

rials showed 3.1 wt% nitrogen; the molar content of viologen groups was calculated to be 1.12 mmol g^{-1}.

Examining the materials by screening reaction times, we found that the relatively tiny and flexible tubular materials formed in the early stage became gradually thicker during the reaction (Supporting Information, Figure S3). Interestingly, when neutral building blocks, such as 4,4‴-diiodo-*p*-quaterphenyl and 4,4″-diiodo-*p*-terphenyl, were used instead of *N*,*N*′-di(4-iodophenyl)-4,4′-bipyridinium chloride, tubular materials were not obtained (Supporting Information, Figure S4). Furthermore, using only toluene or only methanol as solvents, amorphous powders were formed. More extensive studies are definitely required to elucidate the mechanism and will be presented in due course.

Considering the porosity and well-defined outer shape of the MONT, we tested it as a template for secondary inorganic materials. The most interesting case was the reaction with MONT with iron carbonyl (Figure 3a). When MONT reacted with $[Fe_2(CO)_9]$ at 90 °C for 2 days, uniformly coated iron-MONT composites were formed (Supporting Information, Figure S5). X-ray photoelectron spectroscopy (XPS) on composites revealed that the iron species on MONT with Fe 2p orbital peaks at 711.0 eV and 724.4 eV are close to iron oxide formed through air oxidation (Supporting Information, Figure S6). Heat treatment of the isolated iron oxide-MONT composites at 500 °C for 5 h in air resulted in formation of Fe_2O_3 nanotubes (FNTs) with (97 ± 14) nm average diameter (Figure 3b,c). Elemental analysis by combustion revealed that carbon species were completely removed in the FNT. Figure 3e shows a PXRD pattern of the FNT in which all peaks matched well with γ-Fe_2O_3 (JCPDS no. 39-1346) and α-Fe_2O_3 (JCPDS no. 87-1166). XPS studies support the formation of Fe_2O_3 species with Fe 2p orbital peaks at 710.9 eV and 724.5 eV (Figure 3e, inset).[11]

A careful investigation of the walls of the FNT revealed that they consist of nanosized particles with (5.9 ± 0.9) nm average diameter (Figure 3c,d). High-resolution TEM analysis showed the crystalline character of γ-Fe_2O_3 particles on the walls with dominant (311) crystal planes (Supporting Information, Figure S7). BET analysis of the FNT showed a 102.1 m^2 g^{-1} surface area and 0.46 cm^3 g^{-1} total pore volume (P/P_0 = 0.978; Supporting Information, Figure S8). Considering the high density (5.2 g cm^{-3}) of Fe_2O_3, this high surface area might result from the particulate wall structure and inner hollow space. It has been known that nanosized Fe_2O_3 particles have superparamagnetic properties.[12] As shown in Figure 3 f, the hysteresis curve of FNT from a superconducting quantum interference device (SQUID) characterization showed typical superparamagnetic behavior with 58 emu g^{-1}

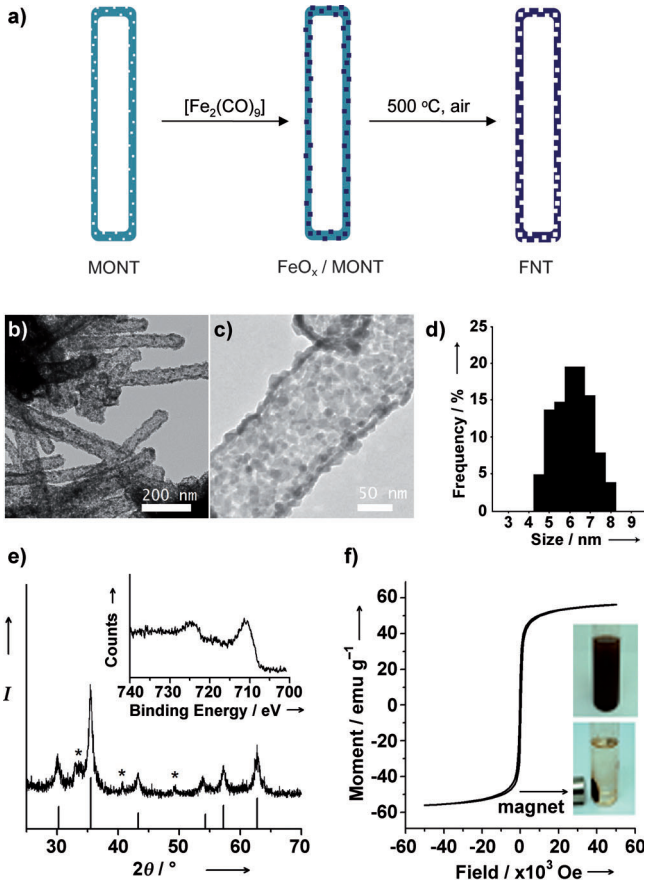

Figure 3. a) Template synthesis of Fe_2O_3 nanotubes (FNTs from MONTs); b–c) TEM images; d) size distribution diagram of Fe_2O_3 particles on a FNT; e) PXRD pattern and simulation of γ-Fe_2O_3 ($\star$ α-Fe_2O_3); inset: XPS spectrum of the Fe 2p orbital; f) hysteresis curve at 298 K and a photograph showing the interaction of the magnet with FNT.

remanent magnetization (M_r) at 298 K, implying that FNTs are magnetically separable in solution chemistry at room temperature.

Iron is the fourth most abundant element on earth's crust, and therefore cheap and non-toxic iron-based materials have attracted the recent attention of scientists for use as energy storage materials.[13] Among iron oxides, Fe_2O_3 usually has four phases, the two main phases being α-Fe_2O_3 (hematite) and γ-Fe_2O_3 (maghemite).[14] Usually, the application of iron oxides as anode materials in lithium ion batteries have focused on α-Fe_2O_3,[15] and studies on γ-Fe_2O_3 as anode materials were relatively little explored.[16] Recently, it has been reported that the desertion of lithium from the lithiated α-Fe_2O_3 resulted in the phase transformation into γ-Fe_2O_3, with reversible Li insertion/desertion in successive cycles.[17] Thus, γ-Fe_2O_3 materials actually showed an identical electrochemical behavior with that of α-Fe_2O_3 from the second charge–discharge process. Moreover, enhanced stabilities of γ-Fe_2O_3 against α-Fe_2O_3 were reported at relatively higher current densities owing to thermodynamic difference of conversion in the first cycle.[17]

One of the notorious problems of iron oxides as anode materials is their rapid loss of discharge capacities during the cycling of lithium ion batteries.[15–17] Recently, the enhanced electrochemical performance of iron oxides has been reported through formation of composites with graphenes.[18] Furthermore, α-Fe_2O_3 hollow spheres were prepared, and these showed enhanced stabilities without the use of graphene, which is possibly due to the structural flexibility originated from the hollow structure.[19] Considering γ-Fe_2O_3 phase and the hollow character, we applied FNTs as anode materials for lithium ion batteries. Using the FNT, coin-type electrochemical cells were fabricated (see the Experimental Section for details). The cells were discharged from open-circuit potential to 1 mV and then cycled between 1 mV and 3 V with a 50 mA g^{-1} current density.

As shown in Figure 4, the FNT showed excellent electrochemical performances with the following four striking features. First, the FNT showed vivid and highly reversible charge–discharge curves (especially from the second cycle), as shown in Figure 4b. It is well-documented that the reversible Li storage process of Fe_2O_3 materials is based on the so-called conversion reaction mechanism and that it undergoes the following electrochemical reaction:[15–17]

$$Fe_2O_3 + 6\,Li^+ + 6\,e^- \leftrightarrow 2\,Fe + 3\,Li_2O$$

The vivid plateau at 0.86 V (vs. Li/Li^+) in the discharge curves, corresponding to reduction of Fe_2O_3 to form Fe^0 and Li_2O, matches well with the reported behavior of iron oxide materials.[15–17]

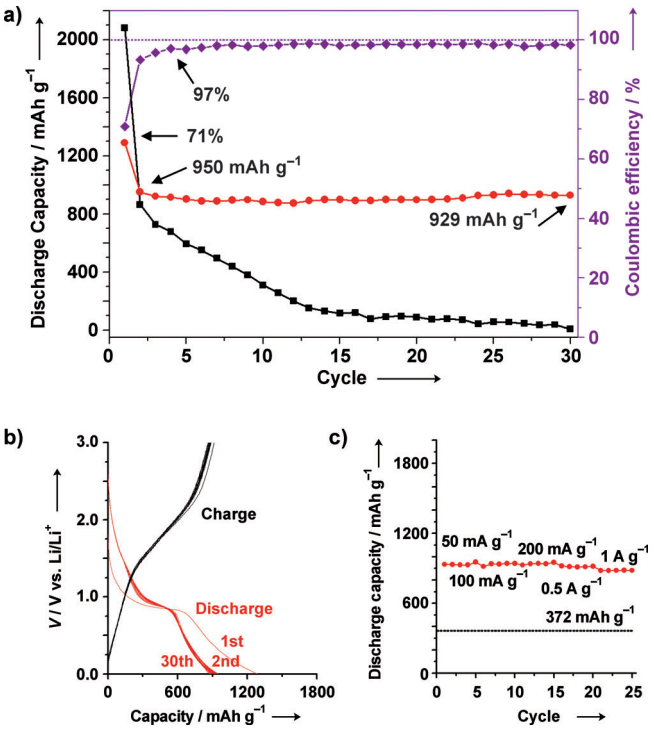

Figure 4. a) Discharge capacities of the FNT (●) and commercial γ-Fe_2O_3 nanoparticles (■) and coulombic efficiencies of FNT (◆) with respect to cycling numbers; b) charge–discharge curves; c) rate performance of the FNT.

Second, the FNT showed a highly reversible discharge capacity of 950 mA h g^{-1} in the second cycle and maintained 929 mA h g^{-1} (97.8% retention of the discharge capacity of the second cycle), even after 30 cycles (Figure 4a). Third, the coulombic efficiency of the FNT at the first cycle was 71%, increased rapidly to 93% at the second cycle, reached 97% at the fourth cycle, and maintained the higher values in successive runs. Iron oxide based anode materials frequently show poor coulombic efficiencies (below 50%) of the first cycle and a relatively large loss of discharge capacities between the first and second cycle.[15–17] Thus, it is quite noteworthy that only a 26% loss of discharge capacities of FNT was observed between the first and second cycles. This excellent performance for the FNT containing mainly the γ-Fe_2O_3 phase is comparable (or better) with the recent best results of non-composite hollow α-Fe_2O_3 materials.[19] In comparison, the commercial iron oxide nanoparticles (5–25 nm average size, primarily γ-Fe_2O_3 phase, Aldrich 544884) showed a rapid loss of discharge capacities during the cycling (Figure 4a; Supporting Information, Figure S9).[20]

Fourth, the FNT showed an excellent rate performance. As shown in Figure 4c, even at 0.5 A g^{-1} and 1 A g^{-1} current densities, the FNT maintained the 918 mA h g^{-1} and 882 mA h g^{-1} discharge capacities, respectively, which are much higher than the maximum discharge capacity (372 mA h g^{-1}) of graphite anode materials. The excellent performance of the FNT might originate from their particulate character and hollow structural feature,[21] which generates the enhanced electrochemical reaction sites and structural flexibility.

In conclusion, through Sonogashira coupling between tetra(4-ethynylphenyl)methane and *N*,*N*′-di(4-iodophenyl)-4,4′-bipyridinium dichloride, microporous organic nanotubes (MONTs) were prepared. The resultant MONTs were used as a template for secondary inorganic materials, namely Fe_2O_3 nanotubes with a high surface area and excellent electrochemical performance as anode materials in lithium ion batteries. This study shows that the synthetic chemistry for microporous organic networks can be applied in development of inorganic energy storage materials. We believe that this approach can be extended for the development of more diverse inorganic electrode materials.

Received: March 21, 2012
Published online: May 24, 2012

Keywords: anode materials · iron oxides · microporous organic networks · nanotubes · Sonogashira coupling

[1] For recent reviews for porous solids, see: a) J. R. Holst, A. I. Cooper, *Adv. Mater.* **2010**, *22*, 5212; b) A. Thomas, *Angew. Chem.* **2010**, *122*, 8506; *Angew. Chem. Int. Ed.* **2010**, *49*, 8328; c) J. Jiang, J. Yu, A. Corma, *Angew. Chem.* **2010**, *122*, 3186; *Angew. Chem. Int. Ed.* **2010**, *49*, 3120.

[2] For selected examples, see: a) S. Che, Z. Liu, T. Ohsuna, K. Sakamoto, O. Terasaki, T. Tatsumi, *Nature* **2004**, *429*, 281; b) P. D. Yang, D. Y. Zhao, D. I. Margolese, B. F. Chmelka, G. D. Stucky, *Nature* **1998**, *396*, 152.

[3] For recent reviews, see: a) O. K. Farha, J. T. Hupp, *Acc. Chem. Res.* **2010**, *43*, 1166; b) C.-D. Wu, W. Lin, *Angew. Chem.* **2007**, *119*, 1093; *Angew. Chem. Int. Ed.* **2007**, *46*, 1075; c) M. Dincă, J. R. Long, *Angew. Chem.* **2008**, *120*, 6870; *Angew. Chem. Int. Ed.* **2008**, *47*, 6766.

[4] For reviews, see: a) J.-X. Jiang, A. I. Copper, *Top. Curr. Chem.* **2010**, *293*, 1; b) A. I. Cooper, *Adv. Mater.* **2009**, *21*, 1291; c) C. Weder, *Angew. Chem.* **2008**, *120*, 456; *Angew. Chem. Int. Ed.* **2008**, *47*, 448; d) M. Mastalerz, *Angew. Chem.* **2008**, *120*, 453; *Angew. Chem. Int. Ed.* **2008**, *47*, 445; e) N. B. Mckeown, P. M. Budd, *Chem. Soc. Rev.* **2006**, *35*, 675.

[5] For selected examples, see: a) N. Du, H. B. Park, G. P. Robertson, M. M. Dal-Cin, T. Visser, L. Scholes, M. D. Guiver, *Nat. Mater.* **2011**, *10*, 372; b) L. Ma, M. M. Wanderley, W. Lin, *ACS Catal.* **2011**, *1*, 691; c) Z. Xie, C. Wang, K. E. deKrafft, W. Lin, *J. Am. Chem. Soc.* **2011**, *133*, 2056; d) J. Weber, A. Thomas, *J. Am. Chem. Soc.* **2008**, *130*, 6334; e) J. Germain, J. M. J. Fréchet, F. Svec, *J. Mater. Chem.* **2007**, *17*, 4989; f) N. B. Mckeown, B. Gahnem, K. J. Msayib, P. M. Budd, C. E. Tattershall, K. Mahmood, S. Tan, D. Book, H. W. Langmi, A. Walton, *Angew. Chem.* **2006**, *118*, 1836; *Angew. Chem. Int. Ed.* **2006**, *45*, 1804.

[6] a) A. M. Shultz, O. K. Farha, J. T. Hupp, S. T. Nguyen, *Chem. Sci.* **2011**, *2*, 686; b) Y.-C. Zhao, D. Zhou, Q. Chen, X.-J. Zhang, N. Bian, A.-D. Qi, B.-H. Han, *Macromolecules* **2011**, *44*, 6382; c) H. C. Cho, H. S. Lee, J. Chun, S. M. Lee, H. J. Kim, S. U. Son, *Chem. Commun.* **2011**, *47*, 917; d) L. Chen, Y. Honsho, S. Seki, D. Jiang, *J. Am. Chem. Soc.* **2010**, *132*, 6742; e) M. Rose, W. Böhlmann, M. Sabo, S. Kaskel, *Chem. Commun.* **2008**, 2462.

[7] a) J.-X. Jiang, F. Su, A. Trewin, C. D. Wood, N. L. Campbell, H. Niu, C. Dickinson, A. Y. Ganin, M. J. Rosseinsky, Y. Z. Khimyak, A. I. Cooper, *Angew. Chem.* **2007**, *119*, 8728; *Angew. Chem. Int. Ed.* **2007**, *46*, 8574; b) J.-X. Jiang, F. Su, A. Trewin, C. D. Wood, H. Niu, J. T. A. Jones, Y. Z. Khimyak, A. I. Cooper, *J. Am. Chem. Soc.* **2008**, *130*, 7710.

[8] a) Y. Inagaki, S. Morishima, K. Wariishi, N. Saito, M. Akiba, *J. Mater. Chem.* **2006**, *16*, 345; b) G. J. Ashwell, G. H. Gross, D. A. Kennedy, I. W. Nowell, J. G. Allen, *J. Chem. Soc. Perkin Trans. 2* **1983**, 1787.

[9] S. Yuan, S. Kirklin, B. Dorney, D.-J. Liu, L. Yu, *Macromolecules* **2009**, *42*, 1554.

[10] Interestingly, even after heating at 700°C for 3 h under argon, the tubular structure was maintained.

[11] X. Teng, D. Black, N. J. Watkins, Y. Gao, H. Yang, *Nano Lett.* **2003**, *3*, 261.

[12] D. Li, W. Y. Teoh, C. Selomulya, R. C. Woodward, P. Munroe, R. Amal, *J. Mater. Chem.* **2007**, *17*, 4876.

[13] For a recent review, see: a) L. Ji, Z. Lin, M. Alcoutlabi, X. Zhang, *Energy Environ. Sci.* **2011**, *4*, 2682; see also: b) P. Poizot, S. Laruelle, S. Grugeon, L. Dupont, J. Tarascon, *Nature* **2000**, *407*, 496.

[14] S. Sakurai, A. Namai, K. Hashimoto, S. Ohkoshi, *J. Am. Chem. Soc.* **2009**, *131*, 18299.

[15] a) Z. Wang, D. Luan, S. Madhavi, Y. Hu, X. W. Lou, *Energy Environ. Sci.* **2012**, *5*, 5252; b) J. S. Chen, T. Zhu, X. H. Yang, H. G. Yang, X. W. Lou, *J. Am. Chem. Soc.* **2010**, *132*, 13162; c) Z. Wang, D. Luan, S. Madhavi, C. M. Li, X. W. Lou, *Chem. Commun.* **2011**, *47*, 8061; d) J. Zhou, H. Song, X. Chen, L. Zhi, S. Yang, J. Huo, W. Yang, *Chem. Mater.* **2009**, *21*, 2935; e) Y. NuLi, R. Zeng, P. Zhang, Z. Guo, H. Liu, *J. Power Sources* **2008**, *184*, 456; f) S. Liu, L. Zhang, J. Zhou, J. Xiang, J. Sun, J. Guan, *Chem. Mater.* **2008**, *20*, 3623; g) J. Chen, L. N. Xu, W. Y. Li, X. L. Gou, *Adv. Mater.* **2005**, *17*, 582.

[16] S. Yamauchi, M. Hibino, T. Yao, *Solid State Ionics* **2011**, *191*, 45.

[17] S. Hariharan, K. Saravanan, P. Balaya, *Electrochem. Solid-State Lett.* **2010**, *13*, A132.

[18] a) X. Zhu, Y. Zhu, S. Murali, M. D. Stoller, R. S. Ruoff, *ACS Nano* **2011**, *5*, 3333; b) G. Zhou, D.-W. Wang, F. Li, L. Zhang, N.

Li, Z.-S. Wu, L. Wen, G. Q. Lu, H.-M. Cheng, *Chem. Mater.* **2010**, *22*, 5306.
[19] B. Wang, J. S. Chen, H. B. Wu, Z. Wang, X. W. Lou, *J. Am. Chem. Soc.* **2011**, *133*, 17146.
[20] Commercial Fe_2O_3 nanoparticles were used (Aldrich, 5–25 nm, primarily γ-Fe_2O_3 phase). The same procedure as that of the FNT was applied to prepare the working electrode.
[21] It is however noteworthy that the hollow nature of anode materials can act as a netgative factor in volumetric discharge capacities.

